AC Quantum Transport Simulation Including Electron-Phonon Scattering

Phil-Hun Ahn and Sung-Min Hong
School of Electrical Engineering and Computer Science (EECS)
Gwangju Insititute of Science and Technology (GIST)
Gwangju, Republic of Korea
smhong@gist.ac.kr

2024 International Conference on Simulation of Semiconductor Processes and Devices (SISPAD) | 979-8-3315-1635-2/24/$31.00 ©2024 IEEE | DOI: 10.1109/SISPAD62626.2024.10733221

***Abstract*—In this work, the small-signal (AC) nonequilibrium Green function (NEGF) simulation results are reported for an extremely scaled MOSFET, including the electron-phonon scattering. Both the AC Poisson equation and the AC NEGF equations are considered by solving a coupled system of equations. The conservation of the AC currents is checked. Moreover, the Y-parameters are obtained at several frequencies. The accuracy of the AC NEGF results is verified by comparing them with low-frequency responses obtained from the DC NEGF.**

I. Introduction

The NEGF simulation [1], [2] is a standard approach to consider the quantum transport in the nanoscale devices. Unfortunately, compared to the conventional technology computer-aided design (TCAD) simulation based on the drift-diffusion model, which allows both steady-state (DC) and AC analyses, the NEGF simulation has been mainly restricted to the DC analysis.

Quite recently, the AC NEGF results for an extremely scaled MOSFET have been reported [3], [4]. It is based on the first-order perturbation of the Poisson equation and the NEGF equations [5], and the current conservation is naturally obeyed. Moreover, the AC response of nanoscale devices is obtained in both low and high frequency ranges. However, in those works, the ballistic transport is assumed, with no scatterings mechanisms included. Extension to a more practical case with the electron-phonon scattering has not been reported yet, even though the formulas are already available in previous works [6].

In this work, for the first time, the AC NEGF simulation results for an extremely scaled MOSFET, including the electron-phonon scattering, is presented. In Section II, relations for the AC NEGF and a coupling scheme for the Poisson equation and the AC NEGF equations are introduced. The simulation results of the AC NEGF are shown in Section III. We demonstrate the verification of our simulation the satisfaction of current conservation. Finally, conclusions are made in Section IV.

II. Methodology

The AC NEGF equations and their implementation are introduced in this section. The AC NEGF equations are briefly shown in Subsection II.A and can also be found in [6]. In Subsection II.B, the fully-coupled scheme for the Poisson equation and the AC NEGF equations is briefly introduced.

A. AC NEGF equations including electron-phonon scattering

The basic equations for the AC NEGF simulation have been reported previously [3], [4], [6], [7]. Only major differences originated from inclusion of the electron-phonon scattering are briefly explained.

In order to include the electron-phonon scattering, scattering self-energies are considered [6], [8]. Both elastic and inelastic scatterings are included in the simulation.

Once the solution of DC NEGF is obtained, the AC NEGF simulation can be performed. An AC voltage excitation with an angular frequency, ω, is assumed to be applied to a contact. AC self-energies for the electron-phonon scattering are again considered as linear terms. Consequently, AC elastic and inelastic scattering self-energies are linearly dependent on the AC lesser, retarded, and advanced Green functions. These self-energies can be written as [6]

$$\begin{aligned}\Sigma^{<}_{AC,inelastic}&(E^+,E)\\ &= \frac{\hbar(D_tK_j)^2}{2\rho\omega_j}[(1+N_q)G^{<}_{AC}(E^+ + \hbar\omega_j, E+\hbar\omega_j)\\ &\qquad + N_q G^{<}_{AC}(E^+ - \hbar\omega_j, E-\hbar\omega_j)],\end{aligned} \quad (1)$$

$$\begin{aligned}\Sigma^{r,a}_{AC,inelastic}&(E^+,E)\\ &= \frac{\hbar(D_tK_j)^2}{2\rho\omega_j}[(1+N_q)G^{r,a}_{AC}(E^+ - \hbar\omega_j, E-\hbar\omega_j)\\ &\qquad + N_q G^{r,a}_{AC}(E^+ + \hbar\omega_j, E+\hbar\omega_j)\\ &\qquad \pm \frac{1}{2}\{G^{<}_{AC}(E^+ - \hbar\omega_j, E-\hbar\omega_j)\\ &\qquad - G^{<}_{AC}(E^+ + \hbar\omega_j, E+\hbar\omega_j)\}],\end{aligned} \quad (2)$$

$$\Sigma^{r,a,<}_{AC,elastic}(E^+,E) = \frac{\Xi^2 k_B T}{\rho u_l^2} G^{r,a,<}_{AC}(E^+,E). \quad (3)$$

For simplicity, notation E^+ is introduced instead of $E+\hbar\omega$, where $\hbar$ is the reduced Planck constant. Terms with subscript j, denoting the phonon index, are related to phonons. The

$$
\begin{pmatrix}
I & & & -L_{V_R G_I^<} & & & & & & & & & & \\
& I & -L_{V_I G_R^<} & & & & & & & & & & & \\
& & I & & & & & & -L_{G_R^< \Sigma_R^<} & -L_{G_R^< \Sigma_I^<} & -L_{G_R^< \Sigma_R^r} & -L_{G_R^< \Sigma_I^r} & -L_{G_R^< \Sigma_R^a} & -L_{G_R^< \Sigma_I^a} \\
& & & I & & & & & -L_{G_I^< \Sigma_R^<} & -L_{G_I^< \Sigma_I^<} & -L_{G_I^< \Sigma_R^r} & -L_{G_I^< \Sigma_I^r} & -L_{G_I^< \Sigma_R^a} & -L_{G_I^< \Sigma_I^a} \\
& & & & I & & & & & & -L_{G_R^r \Sigma_R^r} & -L_{G_R^r \Sigma_I^r} & & \\
& & & & & I & & & & & -L_{G_I^r \Sigma_R^r} & -L_{G_I^r \Sigma_I^r} & & \\
& & & & & & I & & & & & & -L_{G_R^a \Sigma_R^a} & -L_{G_R^a \Sigma_I^a} \\
& & & & & & & I & & & & & -L_{G_I^a \Sigma_R^a} & -L_{G_I^a \Sigma_I^a} \\
& & -L_{\Sigma_R^< G_R^<} & & & & & & I & & & & & \\
& & & -L_{\Sigma_I^< G_I^<} & & & & & & I & & & & \\
& & -L_{\Sigma_R^r G_R^<} & & -L_{\Sigma_R^r G_R^r} & & & & & & I & & & \\
& & & -L_{\Sigma_I^r G_I^<} & & -L_{\Sigma_I^r G_I^r} & & & & & & I & & \\
& & -L_{\Sigma_R^a G_R^<} & & & & -L_{\Sigma_R^a G_R^a} & & & & & & I & \\
& & & -L_{\Sigma_I^a G_I^<} & & & & -L_{\Sigma_I^a G_I^a} & & & & & & I
\end{pmatrix}
\begin{pmatrix}
V_R \\ V_I \\ G_{R,ind}^< \\ G_{I,ind}^< \\ G_{R,ind}^r \\ G_{I,ind}^r \\ G_{R,ind}^a \\ G_{I,ind}^a \\ \Sigma_R^< \\ \Sigma_I^< \\ \Sigma_R^r \\ \Sigma_I^r \\ \Sigma_R^a \\ \Sigma_I^a
\end{pmatrix}
=
\begin{pmatrix}
V_{fixed} \\ 0 \\ G_{R,inj}^< \\ G_{I,inj}^< \\ G_{R,inj}^r \\ G_{I,inj}^r \\ G_{R,inj}^a \\ G_{I,inj}^a \\ 0 \\ 0 \\ 0 \\ 0 \\ 0 \\ 0
\end{pmatrix}
$$

Fig. 1. System of equations for the AC Poisson-NEGF solver. $L_{\alpha\beta}$ denotes the response of α to β. For simplicity, the subscript "AC" is understood. The subscript ind represents "induced" while the subscript inj represents "injected." The injected terms on the right hand-side are related with contact self-energies and injected charges.

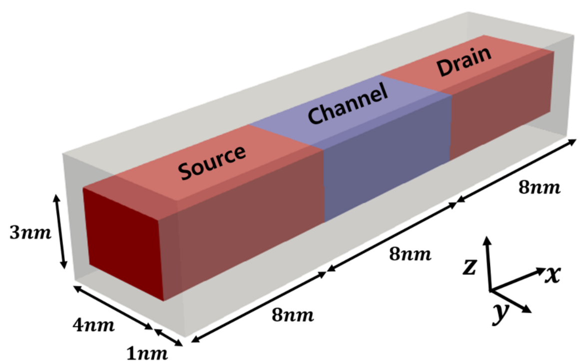

Fig. 2. Nanosheet MOSFET surrounded by a 1-nm-thick oxide layer. Source and drain are doped with a donor concentration of 6×10^{20} cm^{-3}.

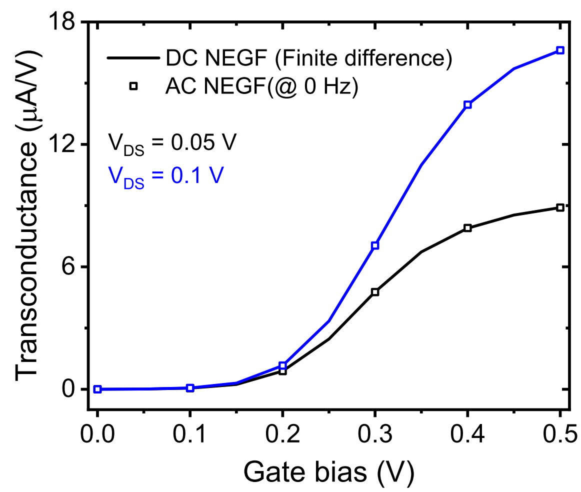

Fig. 3. Transconductance of the nanosheet transistor. The solid lines are finite difference results, while symbols are from the AC NEGF. The drain bias voltage is either 0.05 V or 0.1 V.

retarded and advanced Green functions in (2) and (3) can be obtained as

$$
\begin{aligned}
&G_{AC}^{r,a}(E^+,E) \\
&\quad = G_{DC}^{r,a}(E^+)[V_{AC}(\omega) + \Sigma_{AC,C}^{r,a}(E^+,E) \\
&\qquad + \Sigma_{AC,Scat}^{r,a}(E^+,E)]G_{DC}^{r,a}(E), \quad (4)
\end{aligned}
$$

where V_{AC} is the AC potential energy calculated from the Poisson equation. $\Sigma_{Scat}^{r,a,<}(E^+,E)$ is a total scattering self-energy which is a sum of corresponding elastic and inelastic scattering self-energies. $\Sigma_C^{r,a,<}(E^+,E)$ describes a contact self-energy [3], [4]. As a result, the AC lesser Green function, related with the AC electron density, can be given as

$$
\begin{aligned}
&G_{AC}^<(E^+,E) \\
&= G_{DC}^r(E^+)[\Sigma_{AC,C}^<(E^+,E) + \Sigma_{AC,Scat}^<(E^+,E)]G_{DC}^a(E) \\
&\quad + G_{AC}^r(E^+,E)[\Sigma_{DC,C}^<(E) + \Sigma_{DC,Scat}^<(E)]G_{DC}^a(E) \\
&+ G_{DC}^r(E^+)[\Sigma_{DC,C}^<(E^+) + \Sigma_{DC,Scat}^<(E^+)]G_{AC}^a(E^+,E). \\
&\hfill (5)
\end{aligned}
$$

Once the AC Green functions and AC self-energies are determined, the particle and displacement currents at each terminal can be calculated [6].

B. Implementation

In this subsection, the implementation of AC NEGF equations is briefly introduced. When the ballistic transport is assumed, Green functions and self-energy functions at two different energies are not directly related [4]. Therefore, a compact system of equations [5] is available. On the other hand, when the electron-phonon scattering is included in the simulation, it is no longer allowed to make a compact form of the system matrix.

The resultant system of equations is shown in Fig. 1. L_{Vn} is related to the Poisson equation while the remaining terms are given from the AC NEGF. Each response term can be obtained following a method described in [5], but

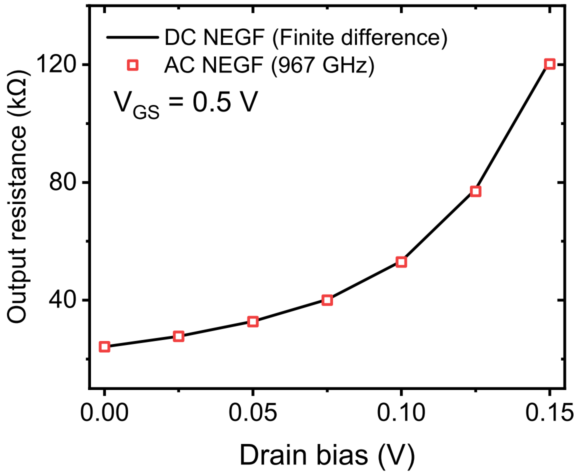

Fig. 4. Output resistance of the nanosheet transistor. The solid line is the finite difference result, while symbols are from the AC NEGF.

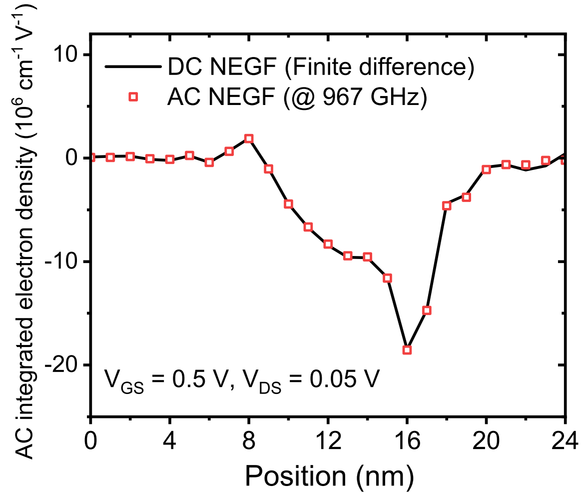

Fig. 6. AC electron density for a drain voltage excitation. The AC NEGF result is calculated at 967 GHz.

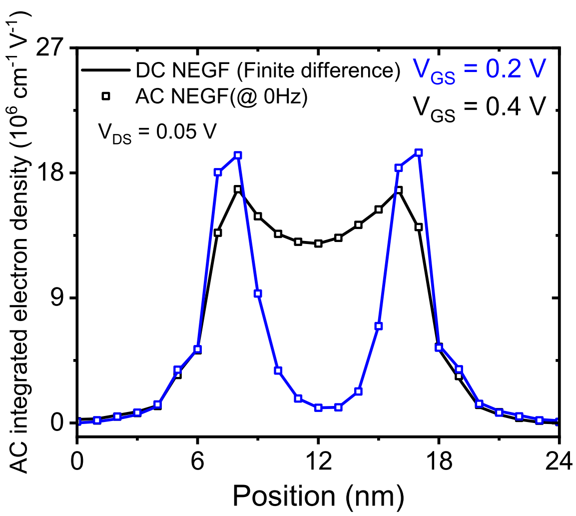

Fig. 5. AC electron density for a gate voltage excitation. The gate bias voltage is either 0.2 V or 0.4 V.

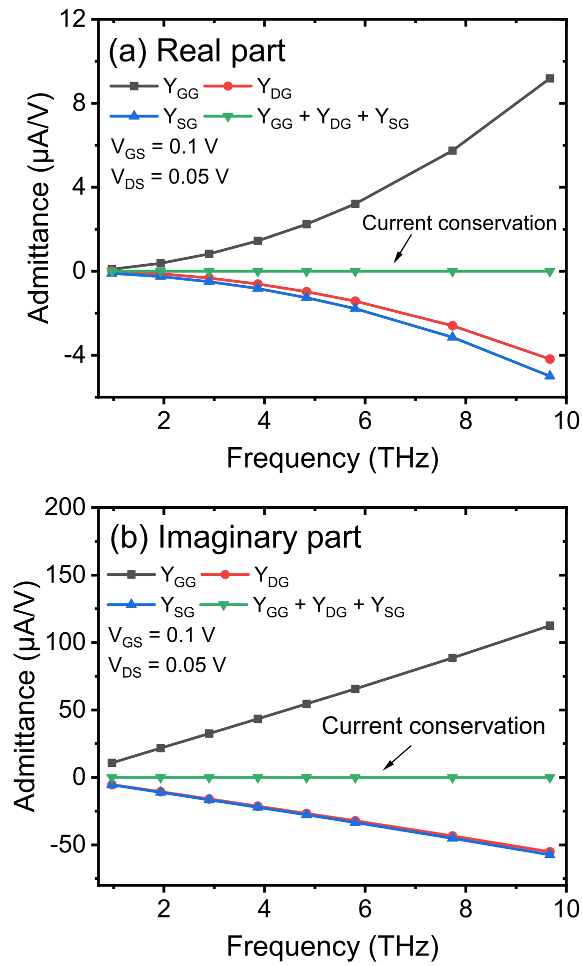

Fig. 7. Y-parameters are drawn as functions of the frequency. The gate voltage excitation is assumed. The total sum of admittances vanishes at every frequency. The frequency varies from 900 GHz to 9 THz. The gate bias is 0.1 V and drain bias is 0.05 V. (a) Real part. (b) Imaginary part.

no energy integration is performed since the Green functions and self-energy functions at two different energies are related. Consequently, each block of response terms becomes larger compared to the ballistic transport case due to the added dependency on the energy grid size. The terms with subscript inj which are at the right-hand side of Fig. 1 are related to the contact self-energies in (4) and (5) and injected charges. On the other hand, the terms with subscript ind are related to the AC potential and scattering self-energies. V_{fixed} specifies the boundary condition.

III. Numerical Results

The AC NEGF simulation is performed for an extremely scaled nanosheet FET. In order to reduce the computational burden in the AC NEGF simulation, we have considered isotropic valleys with the density-of-states effective mass and a relaxed condition for the energy spacing. The nanosheet FET, whose cross-section is 3 nm × 4 nm, is simulated as shown

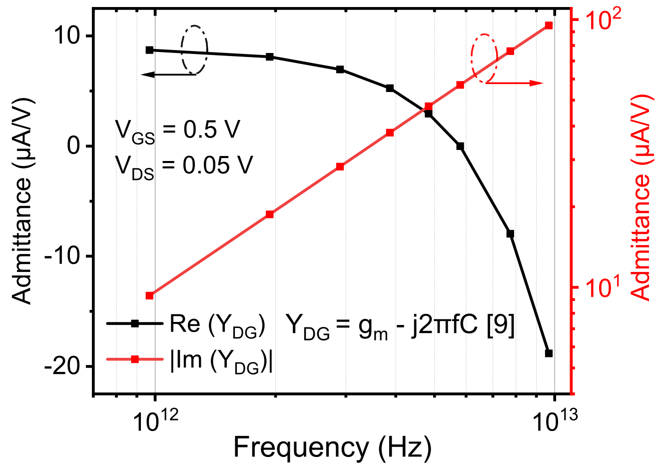

Fig. 8. Real and imaginary parts of Y_{DG} are drawn. V_{GS} = 0.5 V, V_{DS} = 0.05 V.

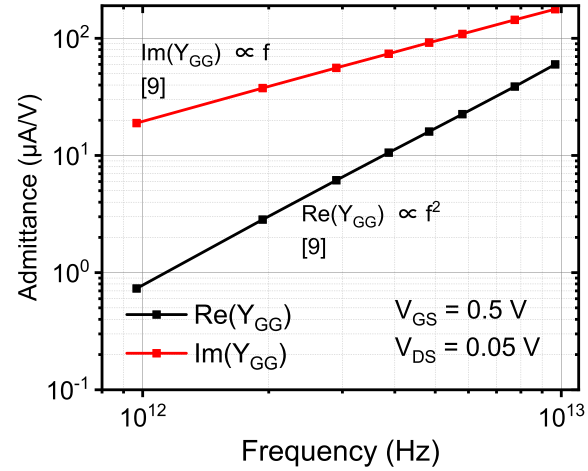

Fig. 9. Real and imaginary parts of Y_{GG} are drawn. V_{GS} = 0.5 V, V_{DS} = 0.05 V.

in Fig. 2. The acceptor doping concentration in the channel is 10^{16} cm^{-3}. Since the real-space NEGF is implemented, a coarse mesh is employed for numerical efficiency. For the electron-phonon scattering, an LO (g-type) inelastic phonon scattering and the elastic scattering are included. [100] channel direction and (001) surface are assumed.

In Figs. 3 and 4, transconductance and output resistance calculated by taking the finite difference of the DC NEGF results are compared with the results from AC NEGF at 0 Hz or at a relatively low-frequency range (967 GHz). For example, the transconductance calculated from the DC NEGF results can be written as

$$g_m = \frac{I_{DC}(V_{GS} + \Delta V) - I_{DC}(V_{GS} - \Delta V)}{2\Delta V}, \qquad (6)$$

where ΔV is a very small voltage difference. A frequency of 967 GHz is related to the energy spacing adopted in the DC and AC NEGF simulation [3]. Both transconductance and output resistance given from the DC NEGF and AC NEGF have good agreement. In Figs. 5 and 6, the AC electron density is compared with the finite difference result. Again, the AC NEGF result given at the low frequency shows a good agreement. In Figs. 3, 4, 5, and 6, we have verified the accuracy of our AC NEGF simulation.

The admittances for the gate voltag excitation at different frequencies are shown in Fig. 7. At each frequency, the current conservation is checked by observing that the total sum of terminal currents vanishes. In Figs. 8 and 9, Y-parameters, Y_{DG} and Y_{GG} are drawn when the frequency varies from 900 GHz to 9 THz. Each Y-parameter matches well with the theoretical equation [9].

IV. Conclusions

In summary, we have shown that the AC NEGF simulation can be performed even with the electron-phonon scattering. Due to the coupling between different energy levels, the system matrix for the AC NEGF simulation becomes much larger than that of the ballistic transport. By comparing the finite difference result from the DC NEGF, the accuracy of our AC NEGF is verified. Moreover, the Y-parameters can be obtained, and the current conservation is also confirmed. As future work, simulation models such as the phonon self-energy, band structure, mesh, numerical efficiency, and so on will be improved for more practical simulation results.

V. Acknowledgement

This research was supported by the National Research Foundation of Korea (NRF) grant funded by the Korea government (NRF-2023R1A2C2007417) and the Samsung Electronics.

References

[1] S. Datta, "A simple kinetic equation for steady-state quantum transport," *Journal of Physics: Condensed Matter*, vol. 2, no. 40, p. 8023, 1990.

[2] ——, "Nanoscale device modeling: the Green's function method," *Superlattices and microstructures*, vol. 28, no. 4, pp. 253–278, 2000.

[3] S.-M. Hong and P.-H. Ahn, "AC NEGF simulation of nanosheet MOSFETs," in *2020 International Conference on Simulation of Semiconductor Processes and Devices (SISPAD)*. IEEE, 2020, pp. 289–292.

[4] P.-H. Ahn and S.-M. Hong, "Quantum transport simulation with the first-order perturbation: Intrinsic AC performance of extremely scaled nanosheet MOSFETs in THz frequencies," in *2021 IEEE International Electron Devices Meeting (IEDM)*. IEEE, 2021, pp. 18–4.

[5] ——, "A fully coupled scheme for a self-consistent Poisson-NEGF solver," *IEEE Transactions on Electron Devices*, vol. 70, no. 1, pp. 239–246, 2022.

[6] Y. Yu, H. Zhan, Y. Wei, and J. Wang, "Current-conserving and gauge-invariant quantum ac transport theory in the presence of phonon," *Physical Review B*, vol. 90, no. 7, p. 075407, 2014.

[7] Y. Wei and J. Wang, "Current conserving nonequilibrium ac transport theory," *Physical Review B—Condensed Matter and Materials Physics*, vol. 79, no. 19, p. 195315, 2009.

[8] J. Charles, P. Sarangapani, R. Golizadeh-Mojarad, R. Andrawis, D. Lemus, X. Guo, D. Mejia, J. E. Fonseca, M. Povolotskyi, T. Kubis *et al.*, "Incoherent transport in NEMO5: realistic and efficient scattering on phonons," *Journal of Computational Electronics*, vol. 15, pp. 1123–1129, 2016.

[9] I. Kwon, M. Je, K. Lee, and H. Shin, "A simple and analytical parameter-extraction method of a microwave MOSFET," *IEEE Transactions on Microwave Theory and Techniques*, vol. 50, no. 6, pp. 1503–1509, 2002.